

# *Ab initio* calculations of excited states in C<sub>4</sub>H and implications for ultraviolet photodissociation

Stephan Graf<sup>a)</sup> and Johannes Geiss

*International Space Science Institute, Hallerstrasse 6, CH-3012 Bern, Switzerland*

Samuel Leutwyler

*Departement für Chemie und Biochemie, Universität Bern, Freiestrasse 3, CH-3012 Bern, Switzerland*

(Received 13 September 2000; accepted 21 December 2000)

Extensive multiconfiguration *ab initio* calculations on the ground state and electronic excited states of the C<sub>4</sub>H radical (butadiynyl) are presented. Using multiconfiguration self-consistent field (MCSCF) structure optimization the estimated complete basis set limit for the excitation energy to the first excited state was calculated to be 0.030 eV employing second-order multireference perturbation theory and 0.035 eV using multireference configuration interaction. States up to 8 eV above the 1<sup>2</sup>Σ<sup>+</sup> ground state were investigated. Harmonic vibrational frequencies for the ground state and the four lowest <sup>2</sup>Π states are reported at the MCSCF level of theory. The 3<sup>2</sup>Σ<sup>+</sup> state is the first state above the C–H bond dissociation threshold at 5.71 eV with a large transition dipole moment, so the 3<sup>2</sup>Σ<sup>+</sup> ← 1<sup>2</sup>Σ<sup>+</sup> transition could lead to dissociation of the C–H bond. The estimated maximum rate for photodissociation is 1.4–3.1 × 10<sup>-6</sup> s<sup>-1</sup> at 1 astronomical unit. Thus C<sub>4</sub>H has a significantly long lifetime in which to be detectable in large parts of cometary comas. © 2001 American Institute of Physics. [DOI: 10.1063/1.1349059]

## I. INTRODUCTION

The butadiynyl (C<sub>4</sub>H) radical occurs in several extraterrestrial objects.<sup>1–19</sup> The first astronomical observation was reported by Guélin *et al.* in the carbon-rich star IRC + 10216.<sup>1</sup> In interstellar molecular clouds (IMCs) the linear radicals C<sub>*n*</sub>H are surprisingly abundant. For instance, in the dark cloud TMC-1, C<sub>4</sub>H was observed to be more abundant than many common molecular species, such as CH<sub>3</sub>CHO, CH<sub>3</sub>OH, HCOOH, CH<sub>3</sub>CN, C<sub>3</sub>H<sub>2</sub>, C<sub>4</sub>H<sub>2</sub>, and HC<sub>3</sub>N. Model calculations<sup>20–22</sup> also predict C<sub>4</sub>H to be among the most abundant organic species, under some IMC conditions even more abundant than H<sub>2</sub>CO or all the other C<sub>*n*</sub>H<sub>*m*</sub> with *n* > 1. The C<sub>*n*</sub>H's with an even number of C atoms have systematically higher abundances than those with an odd number of C atoms. This odd–even effect and a particularly high C<sub>4</sub>H abundance are also predicted by theory, possibly resulting from a carbon insertion process.<sup>20</sup>

Recently the abundance of C<sub>4</sub>H was reported in the coma of Halley's comet.<sup>23</sup> The existence of this radical was derived from the ion abundance data obtained by a ion mass spectrometer (IMS) that, on the Giotto spacecraft, encountered the Halley comet at a solar distance of 0.9 astronomical unit (AU) on 13/14 March 1986. An abundance relative to water of (2.3 ± 0.8) × 10<sup>-3</sup> was reported,<sup>23</sup> which is similar to the abundance of C<sub>2</sub>H<sub>2</sub> or C<sub>2</sub>H<sub>4</sub>.<sup>24</sup> The observation cannot be readily explained by photodissociation of heavier organic molecules, because beyond molecular weight 46 the abundances decrease rapidly.<sup>25</sup> It was concluded<sup>23</sup> that the observed C<sub>4</sub>H was either incorporated in the ice of the nucleus

or it was in some form weakly bound in grains or heavier molecules that were destroyed in less than 10<sup>3</sup> s.

Before the astronomical observations of C<sub>4</sub>H, optical and electron spin resonance (ESR) spectra were measured in rare gas matrices;<sup>26</sup> later laboratory results were obtained in the gas phase and in rare gas matrices.<sup>27–32</sup> These observations and experiments stimulated *ab initio* theoretical work,<sup>8,33–35</sup> and structure optimizations and excited state calculations were performed using Hartree–Fock calculations<sup>36,37</sup> and correlated methods.<sup>30,38–42</sup> In contrast to C<sub>2</sub>H and C<sub>6</sub>H for which there is no dispute as to the symmetry of the ground state, <sup>2</sup>Σ<sup>+</sup> and <sup>2</sup>Π, respectively, the energy difference between these two states in C<sub>4</sub>H is very sensitive to the method chosen. Most authors<sup>30,38,40,42</sup> found the <sup>2</sup>Σ<sup>+</sup> state to be the ground state, in agreement with experimental findings.<sup>26,30</sup>

The relatively high abundance of the C<sub>4</sub>H radical found in the Halley comet raises the possibility that its origin can be traced back to the IMC from which the solar system formed 4.6 billion years ago. It is generally accepted that the high deuterium content in condensable molecules of meteorites and comets is a result of the ion–molecule chemistry in this ancient IMC. Moreover, various lines of evidence indicate that a large fraction of the more refractory grains released by comets is probably of interstellar origin.<sup>43</sup> However, at first it seems surprising that a radical like C<sub>4</sub>H could have survived for 4.6 billion years, even under the very low temperature conditions that prevailed in the comet nucleus throughout its lifetime. In order to better understand the relationship between the butadiynyl in IMCs and in comets we have performed *ab initio* calculations of the ground state and excited states of C<sub>4</sub>H and have investigated various aspects of the chemical and physical properties of this radical.

<sup>a)</sup>Electronic mail: stephan.graf@iss.unibe.ch

TABLE I. Optimized bond lengths (in Å), energies (in  $E_h$ ), and rotational constants  $B_e$  (in GHz) for the ground and first excited states of C<sub>4</sub>H. Structures were optimized at the MCSCF level.

Basis set	Bond				Energy			Rotational constant $B$
	H-C <sub>1</sub>	C <sub>1</sub> -C <sub>2</sub>	C <sub>2</sub> -C <sub>3</sub>	C <sub>3</sub> -C <sub>4</sub>	MCSCF	CASPT2	MRCI+Q	
Ground state $1^2\Sigma^+$								
<i>cc-pVDZ</i>	1.0626	1.2171	1.3844	1.2225	-151.973 956	-152.304 198	-152.339 332	4.6810
<i>cc-pVTZ</i>	1.0527	1.2057	1.3778	1.2109	-152.012 063	-152.437 713	-152.468 571	4.7517
<i>cc-pVQZ</i>	1.0527	1.2046	1.3778	1.2096	-152.021 271	-152.481 265	-152.506 658	4.7569
Est. CBS limit	1.0527	1.2044	1.3778	1.2095	-152.024 204	-152.502 350	-152.522 573	4.7576
Experiment	1.055 <sup>a</sup>	1.215 <sup>a</sup>	1.359 <sup>a</sup>	1.224 <sup>a</sup>				4.7587 <sup>b</sup>
First excited state $1^2\Pi$								
<i>cc-pVDZ</i>	1.0632	1.2288	1.3527	1.2984	-151.960 199	-152.303 400	-152.339 860	4.5896
<i>cc-pVTZ</i>	1.0534	1.2175	1.3447	1.2868	-151.996 902	-152.436 598	-152.468 120	4.6620
<i>cc-pVQZ</i>	1.0534	1.2164	1.3445	1.2854	-152.005 847	-152.480 121	-152.505 708	4.6678
Est. CBS limit	1.0534	1.2163	1.3445	1.2852	-152.008 729	-152.501 245	-152.521 289	4.6684

<sup>a</sup> $r_s$  structure from Ref. 30.<sup>b</sup> $B_0$  see Ref. 4.

The theoretical methods applied are summarized in Sec. II. The optimized structures for the ground state and for the four lowest excited  $2^2\Pi$  states are presented in Sec. III A. Harmonic vibrations of these states will be discussed in Sec. III B and in Sec. III C excitation energies and transition moments from the ground state to various excited states will be reported. Using these results and the solar photon flux, photodissociation rates for C<sub>4</sub>H are estimated in Sec. III D.

## II. METHODS

The basis sets employed for most of this study are the first three members of Dunning's correlation consistent basis sets:<sup>44</sup> *cc-pVDZ*, *cc-pVTZ*, and *cc-pVQZ* (hereafter also *vdz*, *vtz*, and *vqz*). The smallest basis set uses 61 contracted basis functions for the C<sub>4</sub>H radical, increasing to 134 and 250 contracted functions for the *vtz* and *vqz* basis sets. Geometry optimizations were performed at the multiconfiguration self-consistent field (MCSCF)<sup>45,46</sup> level with an active space of nine molecular orbitals (MOs) and nine electrons. This active space consists of the highest singly occupied  $\sigma$  MO, the two occupied  $\pi$  MOs and the lowest two virtual  $\pi$  MOs. The other eight low energy  $\sigma$  molecular orbitals were kept doubly occupied in all configurations, but were allowed to be optimized. The structures for the  $1^2\Sigma^+$  ground state and the first excited state ( $1^2\Pi$ ) were optimized using all three basis sets, whereas the other excited  $\Pi$  states were optimized using the *vtz* basis set only. For the  $\Delta$  and higher  $\Sigma$  electronic states it was necessary to augment the active space described above to 11 or 13 MOs; further details will be given below.

To account for dynamical correlation, second-order multireference perturbation theory (CASPT2)<sup>47</sup> and multireference configuration interaction (MRCI)<sup>48-50</sup> were employed. The MRCI energies including also the multireference Davidson energy correction<sup>51</sup> are labeled MRCI+Q. The reference space used in the CASPT2 or MRCI calculation was generated by a preceding MCSCF step. Depending on the size of the active space in the MCSCF calculation, not all configuration state functions (CSFs) could be included in the reference space. In the case of the smaller active space with 9

MOs, 2068 CSFs are generated for the  $\Sigma$  state and 2352 CSFs for the  $\Pi$  state, respectively. The use of all CSFs in the reference space generated between 3 and 18 million contracted configurations during the CASPT2 calculations (depending on the basis sets and electronic states), which corresponds to 70-170 million uncontracted configurations. In the case of the larger active spaces up to 100 000 CSFs were used in the MCSCF step and the reference space had to be truncated for the subsequent CASPT2 calculation. Selection thresholds of 0.01-0.0005 were applied to the CI expansion coefficients, yielding up to 25 million contracted configurations or up to  $1.6 \times 10^9$  uncontracted configurations.

To check the importance of diffuse functions, especially for the highest-energy states, we extended our calculations to the aug-*cc-pVXZ* ( $X=D$  and  $Q$ ) basis sets. Except for the two highest excited states considered in this study and discussed below, the effects of diffuse functions were very minor.

All calculations were performed using the MOLPRO suite of *ab initio* programs.<sup>52</sup> As MOLPRO uses Abelian point group symmetry only, calculations on linear structures were performed in  $C_{2v}$  instead of  $C_{\infty v}$ . Thus, components of states with different angular momentum belong to the same irreducible representation in  $C_{2v}$ . For example,  $\Sigma^+$  as well as  $\Delta_x^2 - y^2$  occur in the irreducible representation  $A_1$ , in  $B_1$  one obtains  $\Pi_x$  and also  $\Phi_{x^3}$  components. For MCSCF wave functions MOLPRO allows the restriction of  $\Lambda$ , the projection of the angular momentum to the internuclear axis, whereas CASPT2 and MRCI states have to be controlled manually.

## III. RESULTS

### A. Structures and energies

As already mentioned in Sec. II, three basis sets were used for structure optimization. The optimization was done within linear restrictions. Table I presents for the ground state,  $1^2\Sigma^+$ , and first excited state,  $1^2\Pi$ , bond lengths, as well as CASSCF, CASPT2, and MRCI+Q energies. For both ground and excited states, an increase in the basis set size leads to an overall shortening in bond lengths. The

TABLE II. Experimental and theoretical rotational constants (in MHz) for the butadiynyl radical isotopomers and root mean square errors (in MHz) for the theoretical values.

	HCCCC	DCCCC	H <sup>13</sup> CCCC	HC <sup>13</sup> CCC	HCC <sup>13</sup> CC	HCCC <sup>13</sup> C	rms error
Experiment <sup>a,b</sup>	4758.656	4416.441	4614.971	4741.867	4734.633	4594.541	
$r_0^b$	4759.975	4417.592	4616.211	4742.936	4736.206	4595.945	1.30
$r_s^b$	4757.369	4414.864	4613.425	4740.447	4733.511	4593.709	1.32
RCCSD(T) <sup>b</sup>	4707.959	4368.469	4565.731	4690.934	4683.890	4546.521	49.62
RCCSD(T)+corr. <sup>b</sup>	4756.599	4413.015	4612.946	4739.388	4732.256	4593.536	2.34
MCSCF/cc-pVDZ	4681.018	4344.529	4539.600	4664.031	4657.034	4520.518	75.76
MCSCF/cc-pVTZ	4751.724	4410.678	4608.235	4734.377	4727.258	4588.898	6.70
MCSCF/cc-pVQZ	4756.910	4415.393	4613.283	4739.526	4732.388	4593.939	1.73
MCSCF/CBS	4757.567	4415.997	4613.927	4740.177	4733.040	4594.572	1.15

<sup>a</sup>See Ref. 31.<sup>b</sup>See Ref. 30.

lengths show faster convergence for single bonds than for triple bonds. The bond length alternation between single and triple bonds becomes more pronounced with increasing basis set size. Due to the well behaved convergence associated with the use of Dunning's basis sets, it is possible to apply the complete basis set (CBS) scheme to estimate the CBS limit.<sup>53,54</sup> The energy  $E_\infty$  at the CBS limit is obtained from a fit to an exponential function:

$$E(x) = E_\infty + ae^{-bx}, \quad (1)$$

where  $x$  is the cardinal index of the basis set [ $x(vdz)=2$ ,  $x(vtz)=3$ , etc.]. The same function was used for bond length extrapolation and the results are listed in Table I. For comparison with experiments the rotational constants  $B$  including the CBS estimate are also given.  $B$  for the CBS structure is in best agreement with the experimental value, therefore this geometry was used for all transition moment calculations.

The *ab initio* structure shows some differences to the  $r_s$  (substitution structure)<sup>30,55</sup> values for C<sub>4</sub>H. The calculated C–C single bond is 0.019 Å longer, whereas the three other bonds are shorter by 0.002–0.015 Å. Despite these different bond lengths, the calculated rotational constants differ by only 0.2 MHz. Table II shows a comparison of the experimental  $B_0$  rotational constants for six C<sub>4</sub>H isotopomers<sup>30,31,56</sup> with values calculated from *ab initio* structures. The two fitted structures,  $r_0$  and  $r_s$ , show a root mean square (rms) error of 1.3 MHz.<sup>30</sup> Two theoretical structures show rms errors of less than 2 MHz, the *vqz* and CBS structures with 1.7 and 1.2 MHz, respectively. These results show that bond length differences of up to 0.02 Å can reproduce almost the same rotational constants. It is also interesting to note that the theoretical results show excellent agreement with the bond lengths of diacetylene:<sup>57</sup>  $r_{C-H} = 1.0575$  Å,  $r_{C-C} = 1.3729$  Å, and  $r_{C\equiv C} = 1.2095$  Å.

Astonishingly, the MCSCF  $B_e$  converges very close to the experimental  $B_0$  value. This may be due to either a fortuitous cancellation of the terms responsible for the Bastiansen–Morino shrinkage effects,<sup>58</sup> the parallel (anharmonic bond stretching) and perpendicular (bend vibrations) displacements, or the error in the MCSCF structure optimization is equal to the  $r_e - r_0$  difference. In the latter case, two explanations are possible: (i) the MCSCF wave function is not sufficient to describe the C<sub>4</sub>H ground state. This could be

corrected by including additional correlation effects during structure optimization using CASPT2 energies instead of MCSCF only or by increasing the size of the active space for the MCSCF calculation. (ii) The interaction between the ground state and the first excited state is no longer negligible. Improvement in this case would lead to vibronic calculations, which can account for coupling between different electronic states.

On going from the ground state to the first excited state the major structural changes occur at the terminal C<sub>3</sub>–C<sub>4</sub> triple bond, which is elongated by almost 0.08 Å, and at the C<sub>2</sub>–C<sub>3</sub> single bond, which is shortened by 0.03 Å. In the first excited state, the dominant electron configuration changes from  $1\sigma^2, \dots, 8\sigma^2 1\pi^4 2\pi^4 9\sigma$  for the ground state to  $1\sigma^2, \dots, 8\sigma^2 1\pi^4 2\pi^3 9\sigma^2$ . As the  $9\sigma$  MO is antibonding and the  $2\pi$  MO is bonding with respect to the C<sub>3</sub>–C<sub>4</sub> bond, excitation lengthens this bond. The C<sub>2</sub>–C<sub>3</sub> single bond is stabilized because the  $2\pi$  MO, which is antibonding for this C–C bond loses electron population, the  $9\sigma$  MO has no amplitude on this bond.

Table III lists the adiabatic electronic excitation energies for the  $1^2\Pi \leftarrow 1^2\Sigma^+$  transition. The ordering between the  $\Sigma$  and  $\Pi$  states agrees with experiment<sup>32</sup> and several previous *ab initio* studies,<sup>39,40</sup> with the exception of the MRCI+Q result using the smallest basis set, where the  $1^2\Pi$  state lies 0.014 eV lower than the  $1^2\Sigma^+$  state. The reverse order in the MCSCF energies found by Kolbuszewski<sup>40</sup> is not shown by Dunning's basis sets. The estimated CBS limit for the excitation energy was obtained as the difference of the CBS limits of the state energies. The calculated energy difference at the MRCI+Q level between the  $1^2\Sigma^+$  ground state and the first excited  $1^2\Pi$  state is 0.035 eV (3.37 kJ/mol), while the MCSCF calculations overestimate these excitation energies by a factor of 10 or more; see Table III.

TABLE III. Adiabatic electronic excitation energies (in eV) for the  $1^2\Pi \leftarrow 1^2\Sigma^+$  transition of C<sub>4</sub>H.

Basis set	MCSCF	CASPT2	MRCI+Q
<i>cc-pVDZ</i>	0.374	0.022	–0.014
<i>cc-pVTZ</i>	0.413	0.030	0.012
<i>cc-pVQZ</i>	0.420	0.031	0.026
Est. CBS limit	0.421	0.030	0.035

TABLE IV. C<sub>4</sub>H ground state correlation energies  $E_{\text{corr}}$  (in  $E_h$ ) for MCSCF, CASPT2, and MRCI+Q with three different basis sets.  $E_{\text{corr}}$  is defined as the energy difference to the corresponding Hartree-Fock SCF energy,  $E_{vdz} = -151.820\,527\,E_h$ ,  $E_{vtz} = -151.861\,836\,E_h$ ,  $E_{vqz} = -151.871\,298\,E_h$ .

Basis set	MCSCF		CASPT2		MRCI+Q $E_{\text{corr}}$
	$E_{\text{corr}}$	Relative energy <sup>a</sup> (%)	$E_{\text{corr}}$	Relative energy <sup>a</sup> (%)	
<i>cc-pVDZ</i>	0.1534	29.6	0.4837	93.2	0.5188
<i>cc-pVTZ</i>	0.1502	24.8	0.5759	94.9	0.6067
<i>cc-pVQZ</i>	0.1500	23.6	0.6100	96.6	0.6354

<sup>a</sup>Relative correlation energy compared to the corresponding MRCI+Q result.

Table IV shows the correlation energies for the three basis sets at three different levels of theory. One sees that the MCSCF wave function accounts for 30% (*vdz*) to 23% (*vqz*) of the MRCI+Q correlation energy. The MCSCF fraction drops with increasing basis set size because there is an increasing number of virtual orbitals available for electron correlation, which are not included in the constant active space of the MCSCF calculation. Second order perturbation theory recovers more than 93%–97% of the MRCI correlation energy, increasing towards the larger basis sets.

For the <sup>2</sup>Π excited states, a set of optimized structures, listed in Table V, was calculated. These are also used in the harmonic mode analysis (see below). Because a large number of low symmetry calculations are needed in this analysis the *cc-pVTZ* basis was chosen instead of the computationally very demanding quadruple zeta basis set. This decision is justified by the fact that the ground state results in Table V show only minor differences in structures and harmonic mode frequencies between the two basis sets.

There is almost no change in the C–H bond length for the <sup>2</sup>Π excited states; see Table V. The C<sub>1</sub>≡C<sub>2</sub> bond length increases by 0.06 Å in the <sup>2</sup>Π state, and slightly more in the higher excited states. The C<sub>2</sub>–C<sub>3</sub> single bond shortens by 0.03 Å in the <sup>1</sup>Π and <sup>2</sup>Π states and by another 0.06 and 0.02 Å for the <sup>3</sup>Π and <sup>4</sup>Π states, respectively. The largest changes are calculated for the C<sub>3</sub>≡C<sub>4</sub> triple bond. Here the distance increases from 1.21 to 1.40 Å in the <sup>4</sup>Π state. This is the C–C distance corresponding to bond order of 1.5, as in benzene! Also, the dipole moment shows a huge difference between the Σ and the Π states: the excited state dipole moment is at least five times larger than the ground state value.

As will be seen below, not all optimized structures correspond to a local minimum configuration. Further investigations will be needed to search for the global minima of the excited state potential energy surfaces.

## B. Harmonic vibrations

### 1. Ground state

Experimental data for the ground state harmonic vibrations are available from spectroscopy in rare gas matrices<sup>26,29</sup> and anion photoelectron spectroscopy.<sup>59</sup> The IR spectra at 4 K show absorption bands at 2060 and 735 cm<sup>-1</sup>.<sup>26</sup> The first band was attributed to one of the two C≡C stretching modes,  $\nu_2$  (symmetric C≡C stretch) or  $\nu_3$  (antisymmetric C≡C stretch), the second assigned to the C–H bending mode. Strictly speaking, the C<sub>4</sub>H vibrations cannot be labeled as symmetric or antisymmetric but this nomenclature will be used by analogy to the corresponding stretching modes of C<sub>4</sub>H<sub>2</sub>. Shen *et al.*<sup>29</sup> reported the C–H stretching mode  $\nu_1$  at 3307.4 cm<sup>-1</sup> and the C≡C stretching modes at  $\nu_2=2083.9$  cm<sup>-1</sup> and  $\nu_3=2060.6$  cm<sup>-1</sup>. They also claimed that the band at 735 cm<sup>-1</sup> was not due to butadiynyl. This is

TABLE V. C<sub>4</sub>H MCSCF bond lengths (in Å), dipole moments (in debye), and normal mode frequencies (in cm<sup>-1</sup>) for the <sup>1</sup>Σ<sup>+</sup> ground state and the lowest four excited <sup>2</sup>Π states. Ground state properties are calculated using the *cc-pVTZ* and *cc-pVQZ* basis sets, respectively, for the excited states only the *cc-pVTZ* basis set.

Bond lengths			1 <sup>2</sup> Σ <sup>+</sup> a	1 <sup>2</sup> Π	2 <sup>2</sup> Π	3 <sup>2</sup> Π	4 <sup>2</sup> Π
H–C <sub>1</sub>			1.0527	1.0527	1.0538	1.0524	1.0524
C <sub>1</sub> –C <sub>2</sub>			1.2057	1.2046	1.2171	1.2784	1.2845
C <sub>2</sub> –C <sub>3</sub>			1.3778	1.3778	1.3452	1.3489	1.2895
C <sub>3</sub> –C <sub>4</sub>			1.2109	1.2096	1.2859	1.2780	1.3666
Dipole moment			-0.812	-0.802	-4.183	-5.495	-4.521
Vibration		Type	Symmetry				
$\nu_1$	C–H stretch	<i>a'</i>	3607.9	3603.4	3596.1	3601.9	3600.9
$\nu_2$	C≡C symmetric stretch	<i>a'</i>	2301.0	2296.5	2111.8	2179.7	2747.5
$\nu_3$	C≡C antisymmetric stretch	<i>a'</i>	2130.8	2129.3	1905.2	1874.8	1448.0
$\nu_4$	Symmetric stretch	<i>a'</i>	924.1	924.1	907.0	936.1	912.7
$\nu_{5a}$	C–H bend	<i>a'</i>	578.4	575.9	645.3	<i>i</i> 514.3	670.3
$\nu_{5b}$		<i>a''</i>	578.4	575.9	503.5	<i>i</i> 201.4	<i>i</i> 623.2
$\nu_{6a}$	2111 bend	<i>a'</i>	379.3	375.9	2007.3 <sup>b</sup>	502.4	466.4
$\nu_{6b}$		<i>a''</i>	379.3	375.9	441.7 <sup>c</sup>	471.8	342.0
$\nu_{7a}$	221 bend	<i>a'</i>	178.3	178.5	276.2	213.9	163.3
$\nu_{7b}$		<i>a''</i>	178.3	178.5	207.3	214.2	185.4

<sup>a</sup>The first column lists values obtained with the *vtz* basis set and the values in the second column are the results using the *vqz* basis set.

<sup>b</sup>The eigenvector corresponds to the 1211 bend.

<sup>c</sup>The eigenvector corresponds to the 11111 bend.

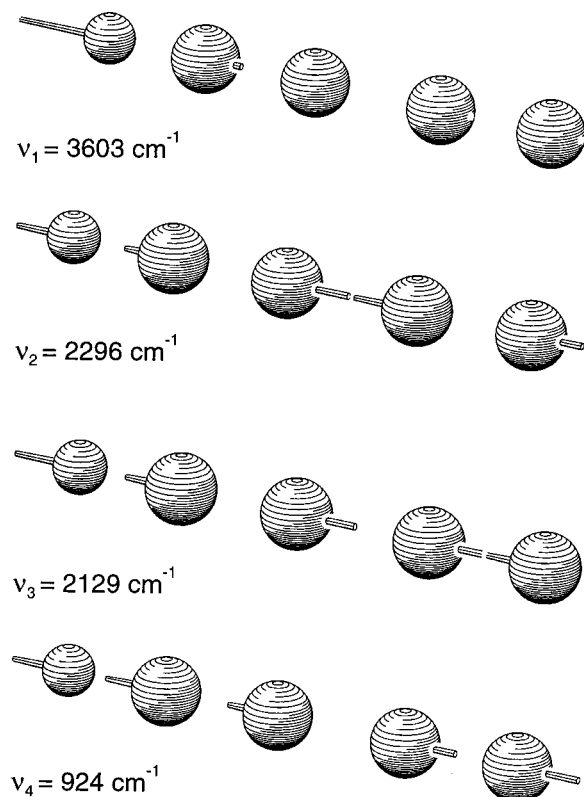


FIG. 1. Normal mode frequencies and eigenvectors of the four stretching vibrations for the  $C_4H$  ground state structure, calculated at the MCSCF/ $cc-pVQZ$  level. For clarity the bonds between atoms within the molecule are omitted and only the Cartesian displacement vectors are given.  $\nu_1$  shows the C–H stretch mode, and  $\nu_2$  and  $\nu_3$  are the symmetric and antisymmetric C≡C stretching vibrations. The lowest mode,  $\nu_4$ , is mainly a C–C stretch.

supported by our calculation of the highest frequency bending mode,  $\nu_5$ , at  $576\text{ cm}^{-1}$  as well as by the results of Kiefer *et al.* with  $\nu_5 = 565\text{ cm}^{-1}$ .<sup>38</sup> The photoelectron spectra of  $C_4H^-$  show peak positions at 226 and  $960\text{ cm}^{-1}$  assigned to the lowest bending mode  $\nu_7$  and the lowest stretching mode  $\nu_4$ , respectively.<sup>59</sup> Also, two combination bands were assigned in these spectra,  $\nu_4 + \nu_7$  at 1186 and  $3065\text{ cm}^{-1}$  for the  $\nu_2 + \nu_4$  combination.

Figures 1 and 2 show the stretching and bending normal mode vibrations for  $C_4H$ . For clarity the four stretching modes in Fig. 1 are shown without bonds between the atoms. The highest frequency mode  $\nu_1$  is assigned to the C–H stretch, the three others are mainly stretching vibration of the C–C triple and single bonds. For the  $\nu_6$  and  $\nu_7$  bending modes we chose labels which count the number of atoms between the nodal points of the normal mode eigenvector, looking from the H atom towards  $C_4$ . The lowest energy bending mode  $\nu_7$  has  $H_1$ ,  $C_1$ , and  $C_4$  moving downward whereas  $C_2$  and  $C_3$  move upward. Thus, there are two nodal points, the first between  $C_1$  and  $C_2$ , the second between  $C_3$  and  $C_4$ , giving the label 221. Modes  $\nu_{5a}$  and  $\nu_{5b}$  could be assigned as the C–H bending modes in all electronic states.

Table V reports normal mode frequencies. For the ground state frequencies calculated with the  $vtz$  and  $vqz$  basis sets are listed. The results show only minor differences of up to a few wave numbers. A comparison of the *ab initio* fre-

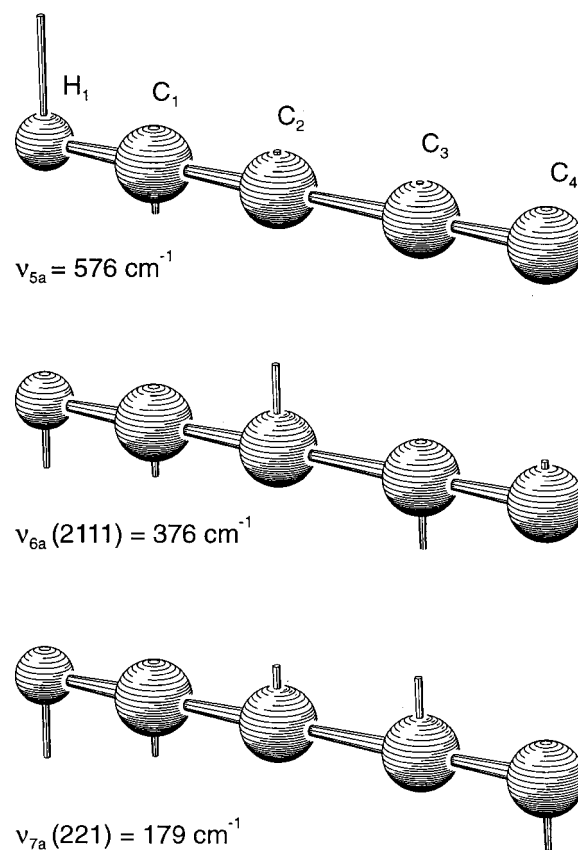


FIG. 2. The three degenerate bending normal modes for the  $C_4H$  ground state structure at the MCSCF/ $cc-pVQZ$  level. Only one component of the degenerated modes is depicted.  $\nu_{5a}$  is the C–C–H bending mode, whereas  $\nu_{6a}$  and  $\nu_{7a}$  represent C–C–C bends. Included in parentheses is also the nodal point nomenclature; see the text.

quencies with the available experimental values shows a difference of 10% at maximum for the stretch vibrations. The frequency of the calculated bend is 21% too low.

## 2. Excited states

Table V also summarizes the normal mode frequencies for four electronic excited  ${}^2\Pi$  states. These frequencies were obtained by numerically differentiating the potential energy with respect to Cartesian coordinates. Due to vibronic interactions (the Renner–Teller effect) in the degenerate  $\Pi$  electronic states, the degenerate  $\pi$  bending vibrations are split into  $a'$  and  $a''$  components. If the Renner–Teller effect is strong, the molecule can deform from a linear structure to lower energy planar (and even nonplanar) structure. According to our calculations this takes place for the  $2^2\Pi$ ,  $3^2\Pi$ , and  $4^2\Pi$  states.

The C–H stretching mode  $\nu_1$  is hardly affected by the electronic state, since all frequencies are within  $12\text{ cm}^{-1}$ . The largest change for  $\nu_2$  occurs in the  $3^2\Pi$  state with a frequency increase of up to  $450\text{ cm}^{-1}$ . The antisymmetric C≡C stretch frequency  $\nu_3$  shows a strong frequency decrease (–30%) with increasing electronic excitation. The frequency of  $\nu_4$  is lower in the excited states than in the ground state, except for  $2^2\Pi$  where it is  $12\text{ cm}^{-1}$  higher. Due to the expected vibronic coupling the bending modes exhibit much larger frequency changes. Very strong splitting occurs for  $\nu_6$

of the  $1^2\Pi$  excited state, which is probably due to interactions with the ground state. To verify this large splitting we distorted the linear structure, shifting the terminal C<sub>4</sub> atom by 0.001 Å in the  $x$  ( $a'$ ) direction. A MCSCF calculation with this structure shows already a mixing of 10% of the  $\Sigma$  wave function into the  $a'$  part of the  $\Pi$  state, whereas the  $a''$  component shows no change. Note that the  $a'$  MO has one electron in the  $xz$  plane and two electrons in the  $yz$  plane; for the  $a''$  MO the occupation is exchanged between both planes. The electronic energy is much more sensitive to structural changes in the plane with one electron.

Only the  $1^2\Pi$  state shows a local minimum at the linear configuration. For the other three excited  $\Pi$  states the linear geometry is a saddle point with a Hessian index of 2 for the  $2^2\Pi$  state and a Hessian index of 1 for the  $3^2\Pi$  and  $4^2\Pi$  states. The negative curvature(s) always arise along the C–H bending coordinate. Due to general occurrence of the Renner–Teller effect, the calculated harmonic bending frequencies represent an estimate for the curvature of the potential energy surface (PES) spectra only. The true vibrational level structure can only be obtained by a vibronic analysis. Therefore it is also not possible to correct the excitation energies for the zero point energy (ZPE).

### C. Vertical excitations

In order to know which states are responsible for photodissociation, calculations of vertical excitation energies and transition moments are important. Due to the  $\Delta\Lambda=0, \pm 1$  selection rules for a linear molecule, mainly excitation to  $\Sigma$  ( $a_1$  symmetry) and  $\Pi$  ( $b_1$  and  $b_2$  symmetries) states are subjects of this study. Nevertheless, analysis of the CI coefficient for some  $a_1$  states leads to an assignment to  $\Delta$  and for some  $b_1/b_2$  states to  $\Phi$  symmetry. The CASPT2 CI coefficients also had to be compared with the corresponding MCSCF calculations since the sequence of the excited states at the CASPT2 level of theory can be different than the sequence at the MCSCF level. For some excited states it was not possible to reach convergence in single state calculations, e.g., the  $2^2\Delta$ . An overview of the CASPT2 vertical excitation energies of the calculated states is given in Fig. 3.

#### 1. $\Pi$ states

Table VI reports the vertical electronic excitation energies  $T_{\text{vert}}$  and squared transition moments from the  $2^2\Sigma^+$  ground state to the first six excited  $2^2\Pi$  states using the  $vdz$ ,  $vtz$ , and  $vqz$  basis sets. All calculations were performed with the CBS ground state structure of C<sub>4</sub>H. All excitation energies  $T_{\text{vert}}$  show good convergence with increasing basis set size, the energy difference between the double  $\zeta$  and the quadruple  $\zeta$  calculations is within a few tenths of an eV. For all states  $T_{\text{vert}}$  is larger for the smaller basis sets compared to in the  $vqz$  results.

To test the reliability of the CASPT2 excitation energies  $T_{\text{vert}}$ , calculations with the  $r_s$  structure<sup>30</sup> for the five lowest  $\Pi$  states were performed. The  $vqz$  results are in Table VII together with the two available experimental values. Using the  $r_s$  geometry lowers all excitation energies, whereas the transition dipole moments show only minor changes. The same is also true for the  $vdz$  and  $vtz$  basis sets (not shown

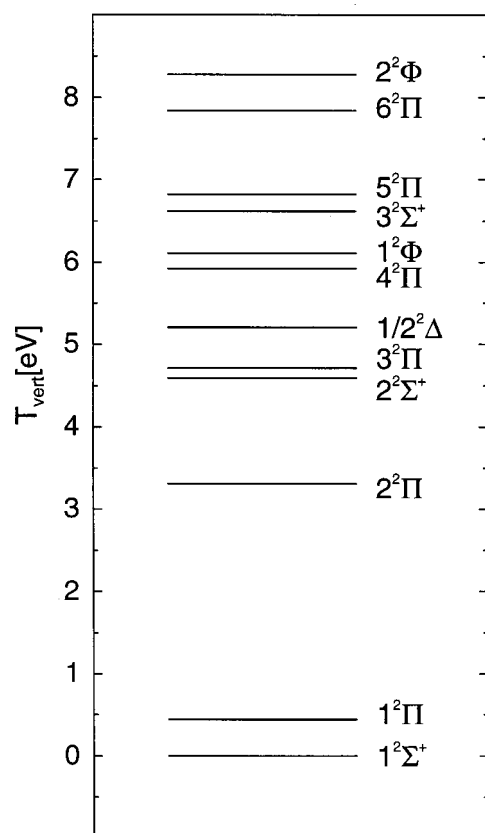


FIG. 3. Vertical excitation energies  $T_{\text{vert}}$  for excited states in C<sub>4</sub>H. All energies were calculated with the  $cc\text{-}pVQZ$  basis set at the CASPT2 level of theory, except for  $3^2\Sigma^+$  where  $cc\text{-}pVTZ$  was used only.

here). Due to this lower  $T_{\text{vert}}$  the difference between the calculated and measured values is reduced from 0.33 to 0.21 eV for the  $2^2\Pi \leftarrow 1^2\Sigma^+$  transition and from 0.52 to 0.21 eV for the  $3^2\Pi \leftarrow 1^2\Sigma^+$  transition. These differences are now within the errors one would expect for CASPT2 calculations.<sup>60–62</sup>

TABLE VI. Vertical electronic excitation energies  $T_{\text{vert}}$  (in eV) and transition moments squared (in D<sup>2</sup>) for excited states in C<sub>4</sub>H. Excitation energies are from CASPT2 calculations at the MCSCF optimized ground state structure.

State	$cc\text{-}pVDZ$		$cc\text{-}pVTZ$		$cc\text{-}pVQZ$	
	$T_{\text{vert}}$	$ \mu_r^2 $	$T_{\text{vert}}$	$ \mu_r^2 $	$T_{\text{vert}}$	$ \mu_r^2 $
$1^2\Pi$	0.52	0.35	0.45	0.37	0.44	0.37
$2^2\Pi$	3.47	0.031	3.32	0.037	3.31	0.038
$3^2\Pi$	5.08	0.021	4.85	0.023	4.71	0.022
$4^2\Pi$	6.29	0.024	6.04	0.018	5.92	0.016
$5^2\Pi$	7.12	0.0021	6.89	0.0031	6.82	0.017
$6^2\Pi$	8.20	0.0068	7.92	0.0063	7.84	0.0063
$2^2\Sigma^+$	4.89(4.84) <sup>a</sup>		4.78(4.70) <sup>a</sup>		4.76(4.59) <sup>a</sup>	
$3^2\Sigma^+$	6.81		6.62			
$1^2\Delta$	5.44		5.26		5.200	
$2^2\Delta$	5.50		5.31		5.205	
$1^2\Phi$	6.23		6.13		6.11	
$2^2\Phi$	8.45		8.31		8.28	

<sup>a</sup>Values in parentheses were obtained from calculations with an active space of 13 orbitals; see the text.

TABLE VII. CASPT2 vertical electronic excitation energies  $T_{\text{vert}}$  (in eV), dominant electron configurations, and squared transition moments  $|\mu_i^2|$  (in D<sup>2</sup>) for the five lowest excited <sup>2</sup>Π states and the two lowest excited <sup>2</sup>Σ<sup>+</sup> states of C<sub>4</sub>H using the experimentally found 1<sup>2</sup>Σ<sup>+</sup> ground state  $r_s$  structure (from Ref. 30). The theoretical results were obtained using the valence quadruple basis sets.

State	Dominant configuration <sup>a</sup>	<i>cc-pVQZ</i>		<i>aug-cc-pVQZ</i>		Expt. $T_0$
		Theoretical $T_{\text{vert}}$	$ \mu_i^2 $	Theoretical $T_{\text{vert}}$	$ \mu_i^2 $	
1 <sup>2</sup> Π	(core) 9σ <sup>2</sup> 1π <sup>4</sup> 2π <sup>3</sup>	0.32	0.35	0.32	0.35	
2 <sup>2</sup> Π	(core) 9σ <sup>2</sup> 1π <sup>3</sup> 2π <sup>4</sup>	3.19	0.040	3.19	0.041	2.98
3 <sup>2</sup> Π	(core) 9σ <sup>2</sup> 1π <sup>4</sup> 2π <sup>2</sup> 3π	4.40	0.020	4.59	0.021	4.19
4 <sup>2</sup> Π	(core) 9σ <sup>2</sup> 1π <sup>4</sup> 2π <sup>2</sup> 3π	5.56	0.016	5.72	0.021	
5 <sup>2</sup> Π	(core) 9σ <sup>2</sup> 1π <sup>3</sup> 2π <sup>3</sup> 3π	6.60	0.015	6.80	0.0017	
2 <sup>2</sup> Σ <sup>+</sup>	(core) 9σ1π <sup>4</sup> 2π <sup>3</sup> 3π	4.42	0.0014	4.53	<4×10 <sup>-5</sup> b	
3 <sup>2</sup> Σ <sup>+</sup>	(core) 9σ1π <sup>3</sup> 2π <sup>4</sup> 3π	6.51 <sup>c</sup>	0.011 <sup>c</sup>	6.61	0.073	

<sup>a</sup>(core)≡1σ<sup>2</sup>,...,8σ<sup>2</sup>.

<sup>b</sup>Not converged; see the text.

<sup>c</sup>Results from *vtz* calculations, because no converged values for the *vgz* basis set were obtained.

Table VII also shows the vertical excitation energies and squared transition moments calculated from the *avgz* basis set. The maximum difference for the excitation energies between both basis sets is only 0.2 eV. The transition dipole moments from the ground state to the 1<sup>2</sup>Π, 2<sup>2</sup>Π, and 3<sup>2</sup>Π states are almost equal for the two basis sets. For the 4<sup>2</sup>Π state, the *avgz* transition dipole moment is 15% larger, whereas for the 5<sup>2</sup>Π state,  $\mu_i(\text{avgz})$  is three times lower.

## 2. Σ, Δ and Φ states

In addition to the above mentioned ground and Π states we did calculations for excited <sup>2</sup>Σ<sup>+</sup>, <sup>2</sup>Δ, and <sup>2</sup>Φ states, the results of which are summarized in Table VI. In order to achieve convergence during the CASPT2 calculation the active space of nine MOs was augmented by up to four additional MOs.

The second Σ state was calculated using a modified active space: we added four σ MOs and removed the 4π MO for a total of 17 electrons in 11 orbitals, five σ MOs (5–9σ), and three π MOs (1–3π). Since no convergence was possible for the third Σ state with this active space, the 4π MO was again included. Even with this huge active space of 13 orbitals it was not possible to achieve convergence for the *vgz* basis set. For comparison the above mentioned large active space with 13 orbitals was also used in the 2<sup>2</sup>Σ<sup>+</sup> calculations; see Table VI. There is an excitation energy difference between the small and the large active space of 0.05–0.17 eV.

The results for the Σ states using the  $r_s$  structure are listed in Table VII. As already seen for the Π states, the effects of diffuse functions on the excitation energies are of the order of 0.1 eV. The *avgz* transition dipole moment for the 3<sup>2</sup>Σ<sup>+</sup>←1<sup>2</sup>Σ<sup>+</sup> transition is 2.6 times larger than the *vtz* value. No convergence was achieved for the transition dipole moment to the 2<sup>2</sup>Σ<sup>+</sup> state with the *avgz* or the smaller *avtz* and *avdz* basis sets.

In between the second and third Σ<sup>+</sup> states the two lowest Δ states were found. As seen in Table VI, the Δ states lie very close together, with the energy gap decreasing with increasing basis set size. These results were obtained using the

active space with 11 MOs. During the calculations for the Π states two pairs of states of  $b_1/b_2$  symmetry but with  $\Lambda = 3$  were found. These wave functions belong to the Φ states in  $C_{\infty v}$ . Although their excitation energies are above the photodissociation threshold, they do not contribute to the dissociation, because Φ←Σ transitions are not dipole allowed.

## D. Photodissociation

Neglecting different electronic states in the products and reactions with three products, there are four possible photodissociation reactions of C<sub>4</sub>H:



Table VIII shows the reaction energies  $\Delta_r E_0$  (electronic energy plus ZPE, calculated at the *G2* level) and the corresponding threshold wavelength. The lowest energy dissociation channel is the C–H bond dissociation, therefore photodissociation is only possible if the molecule is excited to a state at least 5.7 eV above the electronic ground state, neglecting barriers to dissociation.

In the following, we assume that every molecule excited to an electronic state above the dissociation limit will undergo dissociation, typically (but not necessarily) by C–H bond fission, either by direct dissociation, or by predissocia-

TABLE VIII. Reaction energies  $\Delta_r E_0$  (in kJ/mol and eV), corresponding wavelengths, and integrated solar flux of photons above the threshold energy,  $\Phi_{\text{active}}$ , for C<sub>4</sub>H dissociation reactions.

Reaction	$\Delta_r E_0$ (kJ/mol)	(eV)	(nm)	$\Phi_{\text{active}}$ photons/(cm <sup>2</sup> s)
C <sub>4</sub> H→C <sub>4</sub> +H	551	5.71	217.0	4.7×10 <sup>13</sup>
C <sub>4</sub> H→C <sub>3</sub> +CH	567	5.88	210.9	2.4×10 <sup>13</sup>
C <sub>4</sub> H→C+C <sub>3</sub> H	611	6.33	195.9	8.1×10 <sup>12</sup>
C <sub>4</sub> H→C <sub>2</sub> +C <sub>2</sub> H	687	7.12	174.1	1.4×10 <sup>12</sup>

tion following internal conversion to a lower electronic state. At these high energies, bound excited states are usually nonadiabatically coupled to dissociative states, especially along the bending coordinates. We assume that the spontaneous decay rates are low relative to the dissociative mechanisms. Thus, the dissociation rates derived here are upper limits. The absorption rate at a specific wavelength can be expressed as a product of the spectral energy density  $\rho_{\tilde{\nu}}$  and the Einstein coefficient for stimulated absorption,  $B_{\tilde{\nu},ji}$ :

$$k(\tilde{\nu}) = \rho_{\tilde{\nu}} B_{\tilde{\nu},ji}; \quad (6)$$

$\rho_{\tilde{\nu}}$  is proportional to the solar photon flux  $\Phi(\tilde{\nu})$ :

$$\rho_{\tilde{\nu}} = h\Phi(\tilde{\nu}) \frac{\tilde{\nu}}{d\tilde{\nu}}, \quad (7)$$

where  $d\tilde{\nu}$  and  $\tilde{\nu}$  correspond to the width and mean wave number of the selected bin.  $\Phi(\tilde{\nu})$  was taken from Huebner *et al.*,<sup>63</sup> who gave 324 solar flux bins covering a wavelength range from 0 to 14 000 nm at 1 AU.

The Einstein coefficient  $B_{\tilde{\nu},ji}$  is calculated from the *ab initio* transition moment  $\mu_t$ :<sup>64</sup>

$$B_{\tilde{\nu},ji} \left( \frac{m^2}{Js} \right) = \frac{1}{h} G_{ji} (\text{pm}^2) \times 10^{-24} \\ = \frac{1}{h} 41.6238 \mu_t^2 (\text{D}^2) \times 10^{-24}. \quad (8)$$

To model the band shape of the transition we use a Gaussian profile for the absorption band with band center  $\tilde{\nu}_0$  and variable width  $s$ :

$$B_{\tilde{\nu},ji}(\tilde{\nu}) = B_{\tilde{\nu},ji} \frac{1}{\sqrt{2\pi}s} e^{-[(\tilde{\nu}-\tilde{\nu}_0)^2/2s^2]}. \quad (9)$$

In order to simulate different absorption band shapes, the band width  $s$  was varied from 60 up to 4000  $\text{cm}^{-1}$ . The reaction rate is expressed as an integral over this absorption profile:

$$k = \int_{\text{peak}} \rho_{\tilde{\nu}}(\tilde{\nu}) B_{\tilde{\nu},ji}(\tilde{\nu}) d\tilde{\nu}. \quad (10)$$

Figure 4 shows the absorption cross sections  $\sigma_{ji}(\tilde{\nu})$  for different model cases for the  $3^2\Sigma^+ \leftarrow 1^2\Sigma^+$  and the  $5^2\Pi \leftarrow 1^2\Sigma^+$  transitions.

- (1) The *ab initio* excitation energies to the excited states at the optimized ground state structure are used as the band centers, yielding  $T_{\text{vert}}(3\Sigma \leftarrow 1\Sigma) = 6.72$  eV with  $|\mu_t^2|(3\Sigma \leftarrow 1\Sigma) = 0.069$  D<sup>2</sup>, and for the second transition  $T_{\text{vert}}(5\Pi \leftarrow 1\Sigma) = 6.82$  eV.
- (2) Same as (i) but using the experimental  $r_s$  ground state structure, which results in  $T_{\text{vert}}(3\Sigma \leftarrow 1\Sigma) = 6.61$  eV and  $T_{\text{vert}}(5\Pi \leftarrow 1\Sigma) = 6.60$  eV.
- (3) The  $5\Pi \leftarrow 1\Sigma$  excitation energy from (ii) is reduced by 0.21 eV because the calculated excitation energies for  $2^2\Pi$  and  $3^2\Pi$  at the  $r_s$  structure are 0.21 eV too high compared to the experimental results. No correction is made for the  $3\Sigma \leftarrow 1\Sigma$  transition.

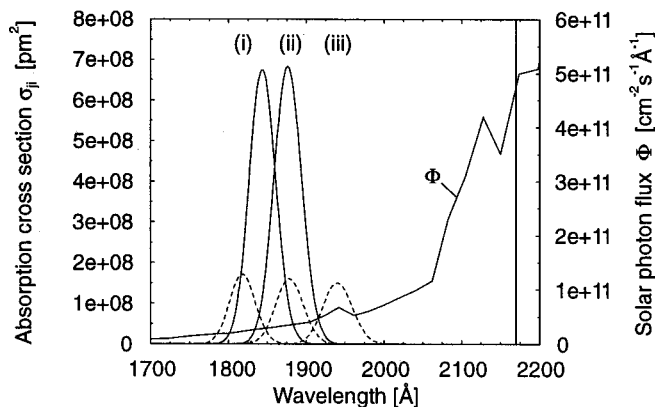


FIG. 4. Calculated absorption cross sections  $\sigma(3^2\Sigma^+ \leftarrow 1^2\Sigma^+)$  (solid line) for two different band center positions using a band width of 500  $\text{cm}^{-1}$  employing the aug-cc-pVQZ basis set. The dashed curves show the calculated absorption cross sections  $\sigma(5^2\Pi \leftarrow 1^2\Sigma^+)$  for three different band center positions using the same band width of 500  $\text{cm}^{-1}$  and employing the cc-pVQZ basis set. (i) Band center is equal to the vertical excitation energy from the ground state to the excited state at the optimized ground state structure, (ii) using the vertical excitation energy at the experimental  $r_s$  ground state structure, (iii) decreasing  $T_{\text{vert}}$  from (ii) by 0.21 eV; also see the text. The solar photon flux  $\Phi$  at 1 AU is also plotted.

For all plots a peak width of  $s = 500$   $\text{cm}^{-1}$  was assumed. Additionally, the solar photon flux at 1 AU is shown together with a vertical bar at 217 nm marking the assumed photodissociation threshold. Note that because of the definition of the integrated absorption cross section,<sup>64</sup>

$$G_{ji} = \int \sigma_{ji}(\tilde{\nu}) \tilde{\nu}^{-1} d\tilde{\nu}, \quad (11)$$

the absorption cross section maximum is lower for the peaks with the band center at larger wavelengths although the transition moment is the same in all three cases.

As the transition dipole moment for the  $5^2\Pi \leftarrow 1^2\Sigma^+$  is almost 10 times lower than that of the  $3^2\Sigma^+ \leftarrow 1^2\Sigma^+$  transition, only the latter was used in the photodissociation rate calculations. Table IX list two sets of values, where the numbers in parentheses are the results from Eq. (10) with integration over the whole absorption band; the other ones are integrated up to 217 nm only. Above this threshold the energy is too low to lead to a photodissociation reaction in C<sub>4</sub>H. Therefore the closer the band center is to this threshold, the larger the differences between both sets of results.

TABLE IX. Estimated photodissociation rates  $k$  (in  $\text{s}^{-1}$ ) at 1 AU for different Gaussian absorption band widths  $s$ . The rates in parentheses are calculated without the cutoff at 217 nm.

$s^a$ ( $\text{cm}^{-1}$ )	Photodissociation rates $k \times 10^6$	
	$T_{\text{vert}}$ (MCSCF structure)	$T_{\text{vert}}$ ( $r_s$ structure)
60	1.4 (1.4)	1.9 (1.9)
125	1.4 (1.4)	1.9 (1.9)
250	1.4 (1.4)	1.9 (1.9)
500	1.4 (1.4)	1.9 (1.9)
1000	1.4 (1.4)	1.9 (1.9)
2000	1.6 (1.6)	2.2 (2.2)
4000	2.4 (3.2)	3.1 (4.7)

<sup>a</sup>The full width at half maximum is 2.35s.

We also neglect an increase of the photodissociation rate due to excitation to higher states, because of the lower photon fluxes. On going from 6 to 7 eV the spectral energy density in the solar spectrum drops roughly by a factor of 10. Although, the corresponding excitation energy to the  $4^2\Pi$  state for case (i) is above the photodissociation threshold, this state is neglected since the excitation energy at the *ab initio* ground state structure is very likely too high, the energies for cases (ii) and (iii) are below the threshold.

Note that the values listed in Table IX are calculated for a quiet sun at a distance of 1 AU. Because the Giotto encounter with comet P/Halley was at 0.9 AU all reaction rates have to be multiplied by a factor of 1.23 to account for the increased photon flux at the smaller distance. The photodissociation rates at 1 AU in Table IX are in the range of  $1.4 \times 10^{-6}$ – $3.1 \times 10^{-6} \text{ s}^{-1}$ . The average of the two limits yields  $k = 2.3 \times 10^{-6} \text{ s}^{-1}$ , corresponding to a lifetime of about  $4.4 \times 10^5 \text{ s}$ . This is comparable to the rate for the proton transfer reaction from  $\text{H}_3\text{O}^+$  to  $\text{C}_4\text{H}$  at a distance of 1000–3000 km from the nucleus of comet P/Halley. Therefore the removal of  $\text{C}_4\text{H}$  is determined by both the photodissociation and the proton transfer reactions.

The traversal time through the inner coma is  $\approx 5500 \text{ s}$ , given by the expansion velocity,  $v_e = 0.8$ – $0.9 \text{ km/s}$  and the distance of the contact surface from the comet's nucleus,  $r = 4600 \text{ km}$ . As both rates are still slow compared to the time needed to traverse the inner coma, only a minor fraction of the neutral  $\text{C}_4\text{H}$  is destroyed. Hence, the  $\text{C}_4\text{H}_2^+$  concentration changes depend mainly on the protonation of  $\text{C}_4\text{H}$  and on the dissociative electron recombination of  $\text{C}_4\text{H}_2^+$ .

A possible alternative source for the  $\text{C}_4\text{H}_2^+$  ion would be the protonation of diacetylene, yielding  $\text{C}_4\text{H}_3^+$ , followed by photodissociation to  $\text{C}_4\text{H}_2^+$ . To model the observed density ratio between mass 50 and 51 of 2.5 at a distance of 2000 km from the nucleus, a very fast photodissociation rate of  $k = 0.0024 \text{ s}^{-1}$  for  $\text{C}_4\text{H}_3^+$  has to be used. To achieve such a high rate excitation to a state close to the dissociation threshold with a transition moment of around 0.5 D would be needed. Only further *ab initio* calculations or experiments could show if such a transition in  $\text{C}_4\text{H}_3^+$  is feasible.

#### IV. CONCLUSIONS

Extensive *ab initio* calculations for the ground state and excited states of  $\text{C}_4\text{H}$  have been presented. Structure optimizations within linear restrictions at the MCSCF level of theory using up to quadruple  $\zeta$  basis sets were performed for the ground and first excited  $1^2\Pi$  states. Comparison between the *vtz* and *vqz* basis sets shows converged bond lengths for the C–H and C–C triple bonds. The *vtz* basis set was also used for structural optimization on the  $2^2\Pi$  to  $4^2\Pi$  states. The excitation energy for the  $1^2\Pi$  state was calculated at the MRCI+Q level of theory and the estimated CBS limit is 0.035 eV, without zero point energy correction. Normal mode analysis for the four lowest  $^2\Pi$  states reveals large Renner–Teller effects; the linear structure is a minimum only for the  $1^2\Pi$  state. For the  $2^2\Pi$ ,  $3^2\Pi$ , and  $4^2\Pi$  states stationary points on the PES with Hessian indices of 2, 1,

and 1 were found. Further relaxation of the optimization restrictions would be needed to find local minimum structures leading to  $C_s$  or  $C_1$  structures.

Some exploratory calculations with augmented basis sets (aug-*cc-pVXZ* with  $X=2,4$ ) were performed. For the  $^2\Pi$  states, the resulting oscillator strengths show only minor changes with respect to those obtained with the *cc-pVXZ* basis sets. The two important exceptions are the transition dipole moments for the  $5^2\Pi \leftarrow 1^2\Sigma^+$  and the  $3^2\Sigma^+ \leftarrow 1^2\Sigma^+$  transitions, which are smaller and larger, respectively.

The lowest-energy photodissociation channel is the C–H bond dissociation, with a calculated reaction energy of 5.71 eV, which can be increased if a barrier exists along the reaction coordinate. Neglecting this, excitation to at least the  $5^2\Pi$  or  $3^2\Sigma^+$  state is necessary for subsequent photodissociation. Excitation to higher states does not contribute significantly to the dissociation rate, due to the lower solar photon flux at shorter wavelengths and smaller transition moments from the ground state to these states. In the reaction rate calculation a single Gaussian peak was used to model the absorption band. The standard deviation of the peak was changed from 60 to  $4000 \text{ cm}^{-1}$ , yielding upper limits to the photodissociation rate between  $1.4 \times 10^{-6}$  and  $3.1 \times 10^{-6} \text{ s}^{-1}$ . Further studies should be directed towards the potential energy curves and curve crossings relevant to the dissociation dynamics of this intermediate size molecule.

#### ACKNOWLEDGMENTS

The authors thank Kathrin Altwegg for advice and discussion and acknowledge support from the ISSI Foundation, the European Space Agency, the Swiss Federation, and the Canton of Berne.

- <sup>1</sup>M. Guélin, S. Green, and P. Thaddeus, *Astrophys. J. Lett.* **224**, L27 (1978).
- <sup>2</sup>P. Friberg, A. Hjalmanson, and W. M. Irvine, *Astrophys. J. Lett.* **241**, L99 (1980).
- <sup>3</sup>W. M. Irvine, B. Höglund, P. Friberg, J. Askne, and J. Elldér, *Astrophys. J. Lett.* **248**, L113 (1981).
- <sup>4</sup>M. Guélin, P. Friberg, and A. Mezaoui, *Astron. Astrophys.* **109**, 23 (1982).
- <sup>5</sup>M. B. Bell, H. E. Matthews, and T. J. Sears, *Astron. Astrophys.* **127**, 241 (1983).
- <sup>6</sup>J. Cernicharo, M. Guélin, and J. Askne, *Astron. Astrophys.* **138**, 371 (1984).
- <sup>7</sup>R. Lucas, A. Omont, S. Guilloteau, and N.-Q. Rieu, *Astron. Astrophys.* **154**, L12 (1986).
- <sup>8</sup>C. A. Gottlieb, E. W. Gottlieb, P. Thaddeus, and J. M. Vrtilik, *Astrophys. J.* **303**, 446 (1986).
- <sup>9</sup>M. Guélin, J. Cernicharo, S. Navarro, D. R. Woodward, C. A. Gottlieb, and P. Thaddeus, *Astron. Astrophys.* **182**, L37 (1987).
- <sup>10</sup>C. A. Olano, C. M. Walmsley, and T. L. Wilson, *Astron. Astrophys.* **196**, 194 (1988).
- <sup>11</sup>N.-Q. Rieu, S. Deguchi, H. Izumiura, N. Kaifu, M. Ohishi, H. Suzuki, and N. Ukita, *Astrophys. J.* **330**, 374 (1988).
- <sup>12</sup>B. E. Turner, *Astrophys. J. Lett.* **347**, L39 (1989).
- <sup>13</sup>J. Bieging and A. Dayal, *Bull. Am. Astron. Soc.* **24**, 1119 (1992).
- <sup>14</sup>Y. Hirahara, H. Suzuki, S. Yamamoto, K. Kawaguchi, N. Kaifu, M. Ohishi, S. Takano, S.-I. Ishikawa, and A. Masuda, *Astrophys. J.* **394**, 539 (1992).
- <sup>15</sup>L.-A. Nyman, H. Olofsson, L. E. Johansson, R. S. Booth, U. Carlstrom, and R. Wolstencroft, *Astron. Astrophys.* **269**, 377 (1993).
- <sup>16</sup>A. Dayal and J. H. Bieging, *Astrophys. J. Lett.* **407**, L37 (1993).
- <sup>17</sup>M. Guélin, R. Lucas, and J. Cernicharo, *Astron. Astrophys.* **280**, L19 (1993).
- <sup>18</sup>S. Fukusaku, Y. Hirahara, A. Masuda, K. Kawaguchi, S.-I. Ishikawa,

- N. Kaifu, and W. M. Irvine, *Astrophys. J.* **437**, 410 (1994).
- <sup>19</sup>M. B. Bell and H. E. Matthews, *Astrophys. J.* **438**, 223 (1995).
- <sup>20</sup>E. Herbst and C. M. Leung, *Astrophys. J., Suppl. Ser.* **69**, 271 (1989).
- <sup>21</sup>H.-H. Lee, E. Herbst, G. Pineau des Forêts, E. Roueff, and J. Le Bourlot, *Astron. Astrophys.* **311**, 690 (1996).
- <sup>22</sup>T. J. Millar, P. R. A. Farquhar, and K. Willacy, *Astron. Astrophys., Suppl. Ser.* **121**, 139 (1997).
- <sup>23</sup>J. Geiss, K. Altwegg, H. Balsiger, and S. Graf, *Space Sci. Rev.* **90**, 253 (1999).
- <sup>24</sup>M. Reber, Ph.D. thesis, University of Bern, 1997.
- <sup>25</sup>A. Korth *et al.*, *Astron. Astrophys.* **187**, 149 (1987).
- <sup>26</sup>K. I. Dismuke, W. R. Graham, and W. Weltner, Jr., *J. Mol. Spectrosc.* **57**, 127 (1975).
- <sup>27</sup>C. A. Gottlieb, E. W. Gottlieb, P. Thaddeus, and H. Kawamura, *Astrophys. J.* **275**, 916 (1983).
- <sup>28</sup>S. Yamamoto, S. Saito, M. Guélin, J. Cernicharo, H. Suzuki, and M. Ohishi, *Astrophys. J. Lett.* **323**, L149 (1987).
- <sup>29</sup>L. N. Shen, T. J. Doyle, and W. R. M. Graham, *J. Chem. Phys.* **93**, 1597 (1990).
- <sup>30</sup>M. C. McCarthy, C. A. Gottlieb, P. Thaddeus, M. Horn, and P. Botschwina, *J. Chem. Phys.* **103**, 7820 (1995).
- <sup>31</sup>W. Chen, S. E. Novick, M. C. McCarthy, C. A. Gottlieb, and P. Thaddeus, *J. Chem. Phys.* **103**, 7828 (1995).
- <sup>32</sup>K. Hoshina, H. Kohguchi, Y. Ohshima, and Y. Endo, *J. Chem. Phys.* **108**, 3465 (1998).
- <sup>33</sup>A. Freeman and T. J. Millar, *Nature (London)* **301**, 402 (1983).
- <sup>34</sup>E. Herbst, *Astrophys. J., Suppl. Ser.* **53**, 41 (1983).
- <sup>35</sup>O. V. Dorofeeva and L. V. Gurvich, *Thermochim. Acta* **197**, 53 (1992).
- <sup>36</sup>S. Wilson and S. Green, *Astrophys. J. Lett.* **212**, L87 (1977).
- <sup>37</sup>F. Pauzat, Y. Ellinger, and A. D. McLean, *Astrophys. J. Lett.* **369**, L13 (1991).
- <sup>38</sup>J. H. Kiefer, S. S. Sidhu, D. Kern, K. Xie, H. Chen, and L. B. Harding, *Combust. Sci. Technol.* **82**, 101 (1992).
- <sup>39</sup>A. L. Sobolewski and L. Adamowicz, *J. Chem. Phys.* **102**, 394 (1995).
- <sup>40</sup>M. Kolbuszewski, *Astrophys. J. Lett.* **432**, L63 (1994).
- <sup>41</sup>J. Natterer and W. Koch, *Mol. Phys.* **84**, 691 (1995).
- <sup>42</sup>D. E. Woon, *Chem. Phys. Lett.* **244**, 45 (1995).
- <sup>43</sup>J. M. Greenberg and A. Li, *Space Sci. Rev.* **90**, 149 (1999), and references therein.
- <sup>44</sup>T. H. Dunning, Jr., *J. Chem. Phys.* **90**, 1007 (1989).
- <sup>45</sup>P. J. Knowles and H.-J. Werner, *Chem. Phys. Lett.* **115**, 259 (1985).
- <sup>46</sup>H.-J. Werner and P. J. Knowles, *J. Chem. Phys.* **82**, 5053 (1985).
- <sup>47</sup>H.-J. Werner, *Mol. Phys.* **89**, 645 (1996).
- <sup>48</sup>H.-J. Werner and P. J. Knowles, *J. Chem. Phys.* **89**, 5803 (1988).
- <sup>49</sup>P. J. Knowles and H.-J. Werner, *Chem. Phys. Lett.* **145**, 514 (1988).
- <sup>50</sup>P. J. Knowles and H.-J. Werner, *Theor. Chim. Acta* **84**, 95 (1992).
- <sup>51</sup>S. R. Langhoff and E. R. Davidson, *Int. J. Quantum Chem.* **8**, 61 (1974).
- <sup>52</sup>MOLPRO is a package of *ab initio* programs written by H.-J. Werner and P. J. Knowles, with contributions by R. D. Amos *et al.*
- <sup>53</sup>D. E. Woon and T. H. Dunning, Jr., *J. Chem. Phys.* **99**, 1914 (1993).
- <sup>54</sup>K. A. Peterson, R. A. Kendall, and T. H. Dunning, Jr., *J. Chem. Phys.* **99**, 1930 (1993).
- <sup>55</sup>H. W. Kroto, *Molecular Rotation Spectra* (Dover, New York, 1992).
- <sup>56</sup>D. R. Woodward, J. C. Pearson, C. A. Gottlieb, and P. Thaddeus, *Astrophys. J. Lett.* **333**, L29 (1988).
- <sup>57</sup>R. Tay, G. F. Metha, F. Shanks, and D. McNaughton, *Struct. Chem.* **6**, 47 (1995).
- <sup>58</sup>S. J. Cyvin, *Molecular Vibrations and Mean Square Amplitudes* (Elsevier, Amsterdam, 1968).
- <sup>59</sup>T. R. Taylor, C. Xu, and D. M. Neumark, *J. Chem. Phys.* **108**, 10018 (1998).
- <sup>60</sup>B. O. Roos, K. Andersson, and M. P. Fülscher, *Chem. Phys. Lett.* **192**, 5 (1992).
- <sup>61</sup>L. Serrano-Andrés, M. Merchán, I. Nebot-Gil, R. Lindh, and B. O. Roos, *J. Chem. Phys.* **98**, 3151 (1993).
- <sup>62</sup>L. Serrano-Andrés, B. O. Roos, and M. Merchán, *Theor. Chim. Acta* **87**, 387 (1994).
- <sup>63</sup>W. F. Huebner, J. J. Keady, and S. P. Lyon, *Astrophys. Space Sci.* **195**, 1 (1992).
- <sup>64</sup>I. Mills, T. Cvitaš, K. Homann, N. Kallay, and K. Kuchitsu, *Quantities, Units and Symbols in Physical Chemistry* (Blackwell Science, Oxford, 1993).